

Super-resolution Optical Fluctuation Imaging—fundamental estimation theory perspective

STANISŁAW KURDZIAŁEK¹ AND RAFAŁ DEMKOWICZ-DOBZAŃSKI^{1*}

¹Faculty of Physics, University of Warsaw, Pasteura 5, PL-02-093 Warszawa, Poland

*Corresponding author: demko@fuw.edu.pl

Compiled September 8, 2020

We provide a rigorous quantitative analysis of super-resolution imaging techniques which exploit temporal fluctuations of luminosity of the sources in order to beat the Rayleigh limit. We define an operationally justified resolution gain figure of merit, that allows us to connect the estimation theory concepts with the ones typically used in the imaging community, and derive fundamental resolution bounds that scale at most as the fourth-root of the mean luminosity of the sources. We fine-tune and benchmark the performance of state-of-the-art methods, focusing on the cumulant based image processing techniques, taking into account the impact of limited photon number and sampling time. © 2020

Optical Society of America

<http://dx.doi.org/10.1364/ao.XX.XXXXXX>

For many years the wave nature of light strictly limited the resolution achievable by optical microscopes. However, over the past 40 years, many techniques, under the common name “super-resolution imaging” [1–20], have been developed to bypass the famous Rayleigh limit [21]. Super-resolution methods can be classified according to the way in which assumptions laying behind the derivation of the traditional resolution limits are broken. Roughly speaking, almost all (far-field) super-resolution techniques can be divided into three groups which are based on (i) sample (light emitters) modification [1–8, 22], (ii) outgoing light measurement modification [9–13] or (iii) illuminating light modification with a particular focus on the use of non-classical states of light [14–19].

Methods (ii,iii) were largely developed by theorists and their fundamental potential and limitations are well understood in terms of quantitative concepts taken from (quantum) information and estimation theories. In particular, by studying basic two (or few) point-sources imaging scenarios, one is able to design the optimal resolving protocols as well as provide rigorous upper-bounds on achievable resolution gains. Still, due to technical challenges the practical impact of these methods is debated and the majority of experimental implementations are proof-of-principle demonstrations rather than versatile imaging systems.

In contrast, methods (i) have been largely developed by experimentalists, are commonly used in modern fluorescent mi-

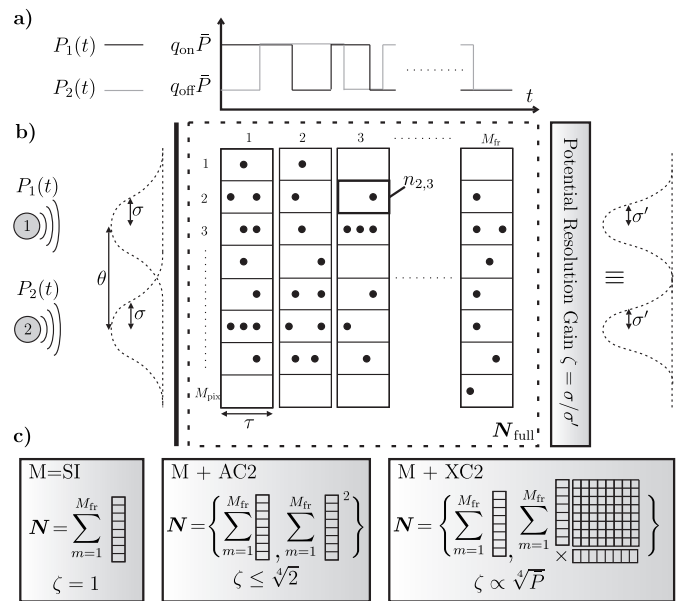


Fig. 1. Imaging model and the overview of the main results. a) Two point sources stochastically switching between two luminosity levels. b) Imaging task reduced to estimation of the point sources separation in the regime of overlapping point-spread-functions. By exploiting the full information N_{full} of number of photons $n_{i,m}$ registered in a given pixel and in a given time-frame of duration τ , it is possible to provide an effective enhancement in resolution compared with the standard imaging where the numbers of photons measured in different time-frames are summed. c) Conceptual representation of different reconstruction methods (utilizing incomplete data N) and the corresponding potential resolution gains ζ : M (mean intensity) = SI (standard imaging), M+AC2 (mean + second temporal auto-cumulant analysis), M + XC2 (mean + cross-cumulant analysis).

croscopy, and are practical for imaging of 2D, or even 3D samples with an arbitrarily complex distribution of emitters. A significant portion of these methods make use of temporal correlations of intensity of each emitter. In methods such as SOFI [5], STORM [3], and PALM [2], positive temporal correlations, explainable by a classical model of emitters with fluctuating

brightness, are utilized. Negative, inherently quantum correlations (anti-bunching) can be used to obtain super-resolution as well [7, 22]. Despite their practical relevance, methods (i) have not been given as much estimation-theoretical attention as methods (ii-iii), see [23] for some notable exception. The goal of this paper is to fill in this gap.

One of the main challenges in approaching imaging problems using the estimation theory perspective is the complexity of the imaging task when viewed as a multiple-parameter estimation problem [24, 25]. As a result, an estimation based approach is often restricted to some rudimentary scenarios where e.g. the problem of estimating the separation between two point sources is considered [9, 23]. An important contribution of this letter is a proposal of the operationally meaningful quantity that can be studied within such a rudimentary scenario and which can be related with the *effective* Point Spread Function (PSF) narrowing, which is a much more appealing concept for people working with practical imaging problems.

Thanks to this connection, it is possible to properly account for the effects of noise, among which the most fundamental is the shot noise resulting from the finite detection statistics. The impact of shot noise is often far from obvious for more sophisticated algorithms of image reconstruction, and, as will be discussed below, cannot be ignored even when dealing with bright sources. Furthermore, when finite detection statistics is combined with the finite correlation times of fluctuating emitters, a non-trivial trade-off in the choice of the optimal sampling time arises—the longer time of a single frame, the better photon statistics, but at the same weaker inter-frame intensity fluctuations.

In order to set the stage for the presentation of the main results, let us start with a brief review of the ideas laying behind the superresolving power of the so called Stochastic Optical Fluctuation Imaging (SOFI) [5], which will be a reference method for the results discussed in this paper. The method is based on calculating temporal cumulants of measured intensity distribution in a number of time frames. It's often claimed, that the resolution can be increased by a factor \sqrt{k} if the k -th cumulant is computed. Let's sketch the argument behind this statement briefly. If the imaged sample consists of L independently fluctuating point emitters, then the light intensity observed in the image plane is:

$$I(\vec{r}, t) = \sum_{i=1}^L P_i(t) U(\vec{r} - \vec{r}_i), \quad (1)$$

where $P_i(t)$ is a stochastic process representing the fluctuating brightness of i -th emitter, \vec{r}_i the position of the emitter in the image plane, and $U(\vec{r})$ is the PSF of the system. Using the fact that emitters are independent, one can compute k -th temporal cumulant of the signal (at each \vec{r} separately) as:

$$\kappa_k(\vec{r}) = \sum_{i=1}^L \kappa_k[P_i(t)] U^k(\vec{r} - \vec{r}_i), \quad (2)$$

where $\kappa_k[P_i(t)]$ is the k -th cumulant of the stochastic process $P_i(t)$. The PSF is now replaced by its k -th power. If the standard, Gaussian approximation of the PSF is used, U^k is narrowed by a factor \sqrt{k} compared with U . Unfortunately, it's well known that higher cumulants are more noisy, and it's not possible to achieve the unlimited resolution gain in practice. It's therefore clear, that noise has to be taken into account in order to assess the maximal resolution gain achievable in SOFI. Some analysis

of the impact of noise on the computed cumulants estimators have been made [26, 27], but the studies have not employed estimation theory concepts such as the Fisher information (FI), and did not make an attempt to benchmark the performance of the methods against the fundamental limitations imposed by estimation theory.

In what follows we provide such a rigorous study. In order to obtain a quantitative insight into the problem, we consider the simplest case of imaging a binary object, which consists of two identical point emitters with fluctuating brightness. Those two emitters are assumed to lie on a known axis, so the whole problem becomes 1D. Moreover, we assume that the centroid of the object is also known, and only the distance between emitters (θ) needs to be estimated, see Fig. 1. Given a random vector N that represents the data, distributed according to a probability distribution which is a function of the estimated parameter $p_\theta(N)$, the variance $\text{Var}[\hat{\theta}]$ of any locally unbiased estimator of θ is lower bounded by $(\mathcal{F}_{\text{meas}})^{-1}$, where

$$\mathcal{F}_{\text{meas}}(\theta) = \int \frac{1}{p_\theta(N)} \left(\frac{\partial p_\theta(N)}{\partial \theta} \right)^2 dN \quad (3)$$

is the FI associated with the whole measurement [28]. For the purpose of comparing different strategies we will use the FI per photon $\mathcal{F}(\theta) = \mathcal{F}_{\text{meas}}(\theta)/\bar{N}$, where \bar{N} is the mean number of photons involved in the experiment.

From now on, we assume that the PSF is Gaussian with standard deviation σ . In this case the FI per one photon as a function of θ for standard imaging (SI) of Poissonian sources with constant brightness $\mathcal{F}^{(\text{SI})}$ [9, 23] (see also Sec. 1.A in Supplement 1) is sketched in Fig. 2, where a significant drop in estimation precision below the Rayleigh limit is visible. In super-resolution microscopy we are mostly interested in the sub-Rayleigh regime, i.e. we assume that $\theta \ll \sigma$. If no noise apart from shot noise is present, and the effect of finite spatial resolution of the detector is neglected, $\mathcal{F}^{(\text{SI})}$ for small θ can be approximated as

$$\mathcal{F}^{(\text{SI})}(\theta) = \mathcal{F}^{(\text{M})}(\theta) = \theta^2/8\sigma^4 + \mathcal{O}(\theta^4/\sigma^6), \quad (4)$$

where we have also indicated that SI is equivalent to the analysis based only on the mean of the total number of photons (M) collected over the whole duration of the imaging experiment. Now it's clear, that if the PSF is narrowed by a factor s , the FI in the limit $\theta \rightarrow 0$ increases by a factor s^4 —this observation allows us to connect PSF-size approach with a more fundamental estimation theory approach. Let's assume that a given super-resolution imaging scheme leads to an increase of FI from $\mathcal{F}^{(\text{SI})}(\theta)$ to $\mathcal{F}(\theta)$. For $\theta \ll \sigma$ this change is equivalent to narrowing the of the PSF by a factor

$$\zeta = \lim_{\theta \rightarrow 0} \left(\mathcal{F}(\theta) / \mathcal{F}^{(\text{SI})}(\theta) \right)^{1/4}. \quad (5)$$

The factor ζ will be called the Potential Resolution Gain (PRG) and will serve us as a figure of merit to assess the performance of different super-resolution methods. Admittedly, it does not contain all the information on the performance of a given super-resolving technique, as it does not capture the performance of the method for larger θ , see Fig. 2. Nevertheless, this quantity captures in a simple way the essence of the super-resolving potential in a basic two point sources model, and allows to compare different methods in a well defined way. Moreover, this quantity also provides us with a meaningful upper bound on

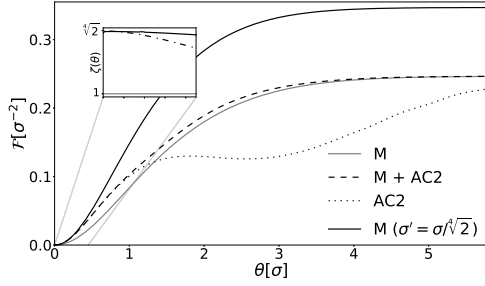


Fig. 2. The FI associated with standard imaging/mean intensity analysis (M) of two point sources is compared with the FI obtained after adding 2nd temporal cumulant to the estimation scheme (M+AC2), and the FI based on 2nd auto-cumulant only (AC2). For small distance θ , very bright emitters, and strong brightness fluctuations, both described improvements are equivalent to narrowing the PSF by $\zeta = \sqrt{2}$. Pixel size $\Delta x = 0.5\sigma$ is assumed.

the performance of a method in more complex imaging scenarios, as discrimination of binary objects is a prerequisite for resolving multiple sources. Interestingly, even such an optimistic bound turns out to be lower than the resolution gain predicted by the naive PSF size analysis in some cases. Finally, maximization of ζ in a given protocol can be regarded as a rule of thumb prescription on the choice of parameters that is likely to lead to the optimal performance of the protocol in real-life scenarios.

For the binary source considered, we fix the positions of the emitters to be $-\theta/2$ and $\theta/2$. Both emitters are statistically identical and independent. Fluctuations of a single emitter brightness are described by a stationary Markov process with two possible relative brightness levels q_{on} and q_{off} satisfying $q_{\text{on}} + q_{\text{off}} = 1$, and $0 \leq q_{\text{off}} \leq q_{\text{on}}$. Such a description leads to exponential distributions for the occupation time of two states, which is observed for many typical dyes [29], and can be used to approximate the QDs power-law blinking [30]. Two states have lifetimes equal to τ_{on} and τ_{off} respectively—in the examples studied we will set $\tau_{\text{on}} = \tau_{\text{off}} = \tau_0$ (some results for $\tau_{\text{on}} \neq \tau_{\text{off}}$ are shown in Sec. 2 of Supplement 1) and τ_0 will play the role of an effective unit of time. The number of photons emitted from a single source over a short time δt , for which the relative brightness q_i may be assumed to be fixed, is described by a Poisson distribution with mean $\bar{P}q_i\delta t$, where \bar{P} parameterizes (in units τ_0^{-1}) the average emitter brightness. Light is detected using a camera with a pixel size Δx , the total number of pixels is M_{pix} , no noise apart from shot noise is considered. In the analysed method it's crucial to track the time dependence of the light intensity, so the whole detection time is divided into M_{fr} intervals of length τ , hereinafter called frames. As a result of the whole measurement one obtains a number of photons in each pixel and in each frame $n_{i,m}$, where $i \in \{1, \dots, M_{\text{pix}}\}$ and $m \in \{1, \dots, M_{\text{fr}}\}$ stand for the pixel and the frame label respectively. In principle, θ may now be estimated from raw data N_{full} containing all $n_{i,m}$. At this point, however, we would like to consider scenarios in which particular algorithms of data analysis are used. We therefore construct a random vector N which contains combinations of variables $n_{i,m}$ which are used in a given θ estimation procedure. Given the probability distribution family $p_{\theta}(N)$, \mathcal{F} can be computed using using Eq. (3).

Let's restrict our considerations to vectors N which can be

written in a form

$$N = \frac{1}{M_{\text{fr}}} \sum_{m=1}^{M_{\text{fr}}} v_m, \quad (6)$$

where v_m depends on variables $n_{1,m}, n_{2,m}, \dots, n_{M_{\text{pix}},m}$ only, in the same way for each frame. The simplest possible choice, $v_m = [n_{1,m}, \dots, n_{M_{\text{pix}},m}]^T$, corresponds to the standard imaging approach, in which only the mean (M) value of signal is taken into account. To take advantage of fluctuations it's necessary to extend the vector N . For example, if we choose v_m , which consists of the elements of the form $n_{i,m}^k$ for $i \in \{1, \dots, M_{\text{pix}}\}$, $k \in \{1, 2, \dots, K\}$, it's possible to construct estimators based on the first K auto-cumulants of the signal in each pixel (M+AC1+...+ACK), as well as compute the associated \mathcal{F} . This formalism also allows us to compute \mathcal{F} when we restrict ourselves to the use of 2nd auto-cumulant only (AC2), as in the basic SOFI scheme—the proper choice of v_m is introduced and justified in Sec. 1.C of Supplement 1.

It's known, that the quality of the image in SOFI can be improved if the correlations between different pixels are utilized. In order to study the efficiency of these class of strategies, we will consider vector v_m comprising elements $\{\{n_{i,m}\}, \{n_{i,m}n_{j,m}\}\}$ for $i, j \in \{1, 2, \dots, M_{\text{pix}}\}$. Such a choice allows to compute a covariance estimator for each pixel pair (M+XC2). Note, however, that in a commonly used cross-cumulant based approach of image reconstruction in SOFI, one doesn't use each covariance independently. Instead, the covariances of pairs with the same centroid are summed, and such a sum is treated as a signal located at the given centroid [31] (M+XC2s). In order to investigate, how much information is lost in such a summation, we will also compute \mathcal{F} corresponding to $v_m = [S_{1,m}, S_{3/2,m}, \dots, S_{M_{\text{pix}},m}, n_{1,m}, \dots, n_{M_{\text{pix}},m}]^T$, where $S_{l,m} = \sum_{(i+j)/2=l} n_{i,m}n_{j,m}$.

Note, that the elements of N are in general correlated in a very non-trivial way. However, everything becomes much simpler in the limit $M_{\text{fr}} \rightarrow \infty$. We can then use the extended version of the central limit theorem [32] (valid in our case, when temporal correlations decay exponentially in time) to conclude that N is normally distributed. Consequently, the FI per photon can be computed using the formula involving the mean value μ of the distribution and its covariance matrix Σ only [28]

$$\mathcal{F} = \frac{1}{N} \frac{\partial \mu^T}{\partial \theta} \Sigma^{-1} \frac{\partial \mu}{\partial \theta}, \quad (7)$$

which is valid for $M_{\text{fr}} \rightarrow \infty$ —see Sec. 1.C of Supplement 1 for the details of Σ and μ computation.

We are now ready to compute $\mathcal{F}(\theta)$ for different estimation schemes, and check how the PRG defined in Eq. (5) depends on the parameters of the setup. The way in which the PRG depends on the time of a single frame τ is particularly interesting. If τ is very long ($\tau \gg \tau_{\text{on}}, \tau_{\text{off}}$), then the fluctuations become averaged inside each frame, and can be hardly observed. On the other hand, when τ is too short, information contained in correlations between subsequent frames is lost. In the extreme case in which one photon is detected in a single frame at most, higher cumulants do not provide any extra information compared with the mean value of the signal. Detailed calculations confirm, that $\zeta \rightarrow 1$ in the limit $\tau \rightarrow 0$ and $\tau \rightarrow \infty$, both in the case of auto-cumulant and cross-cumulant based estimation. In order to reach the optimal ζ one needs to avoid both

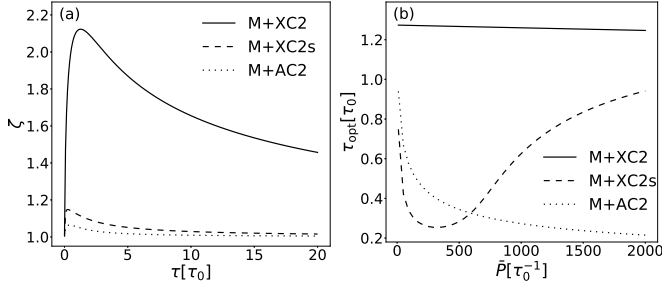


Fig. 3. PRGs for different methods (ζ) depend on the frame time τ in the way shown in (a) (for $\bar{P} = 300\tau_0^{-1}$). Optimal time frame τ_{opt} , for which ζ is maximal, depends on emitters brightness \bar{P} in the way shown in (b). Parameters used: $\tau_{\text{on}} = \tau_{\text{off}} = \tau_0$, $q_{\text{off}} = 0$, $q_{\text{on}} = 1$, $\Delta x = 0.5\sigma$.

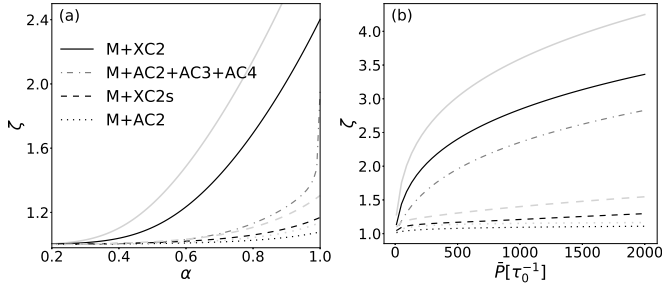


Fig. 4. ζ as a function of α (for $\bar{P} = 500\tau_0^{-1}$) (a), and as a function of \bar{P} (for $\alpha = 1$) (b) is sketched for different estimation schemes. Black lines correspond to results obtained using realistic blinking model, with $\tau_{\text{on}} = \tau_{\text{off}} = \tau_0$, and the optimal choice $\tau = \tau_{\text{opt}}$. Results obtained with the help of simplified model (see the text) with corresponding parameters ($p = 0.5$, $\tau = \tau_0$) are denoted by gray lines. Pixel size: $\Delta x = 0.5\sigma$.

extremes and identify the optimal value of τ , which in general depends on the estimation method and the emitters brightness, see Fig. 3. Note that the cross-cumulant methods tend to benefit from longer frames, which allow to collect more photons and effectively reduce the shot noise of the data, while the auto-cumulant method, with its reduced data complexity, favours shorter frames and as a result stronger effective brightness fluctuations.

Let us now compare different estimation schemes in terms of their PRGs when the optimal frame time $\tau = \tau_{\text{opt}}$ is used in each case. The dependence of PRGs on emitters brightness \bar{P} and fluctuation strength defined as $\alpha = 1 - q_{\text{off}}/q_{\text{on}}$ is shown in Fig. 4. It is clear, that the cross-correlation based approach outperforms auto-cumulant based estimation significantly. Moreover, the relevant part of information is lost if the summation of covariances for pairs with the same centroid is carried out, as in [31]. This indicates a space for improvement in the application of cross-cumulant based methods.

Until now, we have focused on estimation schemes based on 2nd order correlations. Going beyond this approach, we want to establish the fundamental upper-bound on the PRG, ζ_{max} , which doesn't depend on the estimation scheme. To do so, we should compute the FI for a model involving all the data $n_{i,m}$, and moreover, allow both the temporal and spatial resolution of

the detector to be unlimited. This task is computationally much more challenging than the previous one, so in what follows we consider a simplified model of fluctuating sources. Previously, the intervals between subsequent state switches were irregular. Therefore, brightness changes were observed within individual frames, and frames were correlated. From now on, we are going to neglect both of these effects, and assume, that brightness of both emitters are drawn in each frame independently. The relative brightness of each emitter remains constant in each frame, and takes the values $q_{\text{off}}, q_{\text{on}}$ with probabilities $p, 1 - p$ respectively. The number of photons emitted during a single frame from a source with a relative brightness q_i is drawn from the Poisson distribution with mean $q_i\bar{P}\tau$. Let us now check how the described simplification affects our previous results in the particular case in which the on- and off-states are equally probable. It corresponds to $p = 0.5$ in the simplified model, and to $\tau_{\text{on}} = \tau_{\text{off}}$ in the realistic one. Furthermore, we are going to choose our parameters such that the average blinking frequency is the same in both models, i.e. the frame time in the simplified model is equal to emitters lifetimes in the Markov-process-based model ($\tau = \tau_{\text{on}} = \tau_{\text{off}}$). Frame time in the realistic model is assumed to be optimal $\tau = \tau_{\text{opt}}$. As can be seen in Fig. 4, the simplified model tends to overestimate ζ , but qualitatively the dependence of ζ on different parameters as well as ordering of different methods in terms of their performance is unaffected.

Unlimited spatial resolution of the detector means, that our complete data from each frame comprises the list of all the detected photon positions x_1, \dots, x_n (detection times do not provide any extra information in the model). In order to compute the complete-data-based FI one needs to find the probability of measuring a given sequence of photon positions $p_\theta(x_1, \dots, x_n)$ averaged over unknown emitters' brightness. Then, $\mathcal{F}(\theta)$ for θ satisfying $\theta \ll (\bar{P}\tau)^{-1/2}$ can be calculated using Eq. (3) and the corresponding PRG can be written as (see Sec. 1.B of Supplement 1)

$$\zeta_{\text{max}} = \sqrt[4]{1 + G(p, \alpha, \bar{P}\tau)\bar{P}\tau}, \quad (8)$$

where $\alpha = 1 - q_{\text{off}}/q_{\text{on}}$ is the fluctuation strength. Function G is ascending with respect to $\bar{P}\tau$ and is upper-bounded by an expression which does not depend on $\bar{P}\tau$

$$\lim_{\bar{P}\tau \rightarrow \infty} G(p, \alpha, \bar{P}\tau) = \frac{\alpha^4 p(1-p)}{(2-\alpha)^3(1-p\alpha)}. \quad (9)$$

Numerical computations show, that the above limit approximates G with an accuracy better than 1% for $\bar{P}\tau \gtrsim 2500$ in the case of weak fluctuations ($\alpha = 0.2$). G converges much faster for strong fluctuations ($\alpha = 1$) (see Fig. S1 in Supplement 1), then the mentioned accuracy is achieved for $\bar{P}\tau \gtrsim 50$, and the PRG can be approximated as :

$$\zeta_{\text{max}} \simeq \sqrt[4]{1 + p\bar{P}\tau}. \quad (10)$$

We see that $\zeta_{\text{max}} \sim (\bar{P}\tau)^{1/4}$ for large number of photons per frame $\bar{P}\tau$ for different fluctuation parameters. As depicted in Fig. 5, a similar scaling is observed numerically for ζ associated with cross-cumulant based estimation. However, the situation is different if only the mean and the 2nd auto-cumulant of the signal is involved in the estimation scheme, as in this case $\zeta(\bar{P}\tau = \infty)$ is finite. In particular, if we restrict our considerations to the symmetric case $p = 0.5$ (other p values are discussed in Sec. 2 of Supplement 1), no PRG higher than $\sqrt[4]{2}$ can be achieved via this method. This demonstrates, that the resolution gain $\sqrt{2}$ predicted by the PSF narrowing analysis cannot

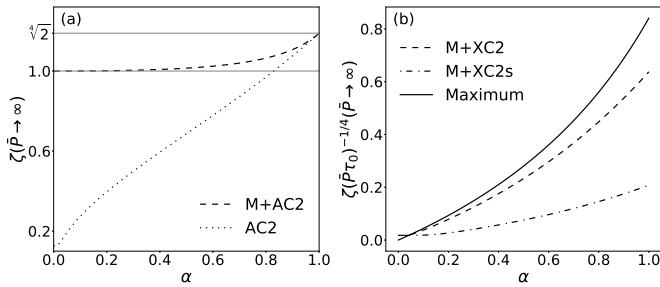


Fig. 5. ζ in the limit $\bar{P} \rightarrow \infty$ associated with estimation schemes based on 2nd auto-cumulant calculated for simplified model as a function of α is shown in (a). For $p = 1/2$ the PRG is never larger than $\sqrt[4]{2}$. Even for large \bar{P} , the replacement of mean with 2nd cumulant is not advantageous, unless fluctuations strength α is large enough ($\zeta < 1$ for $\alpha < 0.83$). Fundamental upper-bound ζ_{\max} , as well as PRGs associated with utilizing cross-cumulants scale as fourth-root of \bar{P} , $\lim_{\bar{P} \rightarrow \infty} \zeta / \sqrt[4]{\bar{P}}$ is sketched in (b).

be achieved even for strong fluctuations, very bright sources and large number of frames. Interestingly, a similar discrepancy (the PRG is $\sqrt[4]{2}$, not $\sqrt{2}$) can be observed for a simple case of anti-bunching based imaging—see Sec. 3 of Supplement 1.

To summarize, we have provided a quantitative approach based on estimation theory, to compute performance limits on super-resolution imaging methods that utilize sources brightness fluctuations. By focusing on the rudimentary problem of resolving two point sources, we were able to provide a single meaningful quantity that allows to compare resolution gain of different methods and identify the optimal detection frame time. The study, has on one hand identified new fundamental limitations of some of the methods (e.g. 2nd auto-cumulant method) as well as indicated space for improvement of other methods (e.g. cross-cumulant based methods). Since the study was based on two point sources imaging problem, the obtained resolution limits can be regarded as signatures of the potential of the methods if applied to more complex multiple sources imaging. A more detailed multiple-parameter based estimation approach may provide a further insight into the potential as well as the limitations of these methods in more complex imaging scenarios.

ACKNOWLEDGEMENTS

We thank Konrad Banaszek for fruitful discussions. We acknowledge support from the National Science Center (Poland) grant No.2016/22/E/ST2/00559.

REFERENCES

- E. Betzig, "Proposed method for molecular optical imaging," *Opt. Lett.* **20**, 237–239 (1995).
- E. Betzig, G. H. Patterson, R. Sougrat, O. W. Lindwasser, S. Olenych, J. S. Bonifacino, M. W. Davidson, J. Lippincott-Schwartz, and H. F. Hess, "Imaging intracellular fluorescent proteins at nanometer resolution," *Science* **313**, 1642–1645 (2006).
- M. J. Rust, M. Bates, and X. Zhuang, "Sub-diffraction-limit imaging by stochastic optical reconstruction microscopy (storm)," *Nat. Methods* **3**, 793–796 (2006).
- S. W. Hell, "Far-field optical nanoscopy," *Science* **316**, 1153–1158 (2007).
- T. Dertinger, R. Colyer, G. Iyer, S. Weiss, and J. Enderlein, "Fast, background-free, 3d super-resolution optical fluctuation imaging (sofi)," *Proc. Natl. Acad. Sci.* **106**, 22287–22292 (2009).
- B. O. Leung and K. C. Chou, "Review of super-resolution fluorescence microscopy for biology," *Appl. Spectrosc.* **65**, 967–980 (2011). PMID: 21929850.
- D. Gatto Monticone, K. Katamadze, P. Traina, E. Moreva, J. Forneris, I. Ruo-Berchera, P. Olivero, I. P. Degiovanni, G. Brida, and M. Genovese, "Beating the abbe diffraction limit in confocal microscopy via nonclassical photon statistics," *Phys. Rev. Lett.* **113**, 143602 (2014).
- W. E. Moerner, "Nobel lecture: Single-molecule spectroscopy, imaging, and photocontrol: Foundations for super-resolution microscopy," *Rev. Mod. Phys.* **87**, 1183–1212 (2015).
- M. Tsang, R. Nair, and X. M. Lu, "Quantum theory of superresolution for two incoherent optical point sources," *Phys. Rev. X* **6**, 031033 (2016).
- M. Paúr, B. Stoklasa, Z. Hradil, L. L. Sánchez-Soto, and J. Rehacek, "Achieving the ultimate optical resolution," *Optica* **3**, 1144–1147 (2016).
- F. Yang, A. Tashchilina, E. S. Moiseev, C. Simon, and A. I. Lvovsky, "Far-field linear optical superresolution via heterodyne detection in a higher-order local oscillator mode," *Optica* **3**, 1148–1152 (2016).
- W.-K. Tham, H. Ferretti, and A. M. Steinberg, "Beating rayleigh's curse by imaging using phase information," *Phys. Rev. Lett.* **118**, 070801 (2017).
- M. Parniak, S. Borówka, K. Boroszko, W. Wasilewski, K. Banaszek, and R. Demkowicz-Dobrzański, "Beating the rayleigh limit using two-photon interference," *Phys. Rev. Lett.* **121**, 250503 (2018).
- S.-H. Tan, B. I. Erkmén, V. Giovannetti, S. Guha, S. Lloyd, L. Maccone, S. Pirandola, and J. H. Shapiro, "Quantum illumination with gaussian states," *Phys. Rev. Lett.* **101**, 253601 (2008).
- A. N. Boto, P. Kok, D. S. Abrams, S. L. Braunstein, C. P. Williams, and J. P. Dowling, "Quantum interferometric optical lithography: Exploiting entanglement to beat the diffraction limit," *Phys. Rev. Lett.* **85**, 2733–2736 (2000).
- M. A. Taylor, J. Janousek, V. Daria, J. Knittel, B. Hage, H.-A. Bachor, and W. P. Bowen, "Subdiffraction-limited quantum imaging within a living cell," *Phys. Rev. X* **4**, 011017 (2014).
- L. A. Rozema, J. D. Bateman, D. H. Mahler, R. Okamoto, A. Feizpour, A. Hayat, and A. M. Steinberg, "Scalable Spatial Superresolution Using Entangled Photons," *Phys. Rev. Lett.* **112**, 223602 (2014).
- J. P. Dowling and K. P. Seshadreesan, "Quantum optical technologies for metrology, sensing, and imaging," *J. Light. Technol.* **33**, 2359–2370 (2015).
- M. Genovese, "Real applications of quantum imaging," *J. Opt.* **18**, 073002 (2016).
- C. Schnell, "Quantum imaging in biological samples," *Nat. Methods* **16**, 214–214 (2019).
- M. Born and E. Wolf, *Principles of optics: electromagnetic theory of propagation, interference and diffraction of light* (Elsevier, 2013).
- O. Schwartz and D. Oron, "Improved resolution in fluorescence microscopy using quantum correlations," *Phys. Rev. A* **85**, 033812 (2012).
- S. Ram, E. S. Ward, and R. J. Ober, "Beyond rayleigh's criterion: A resolution measure with application to single-molecule microscopy," *Proc. Natl. Acad. Sci.* **103**, 4457–4462 (2006).
- S. Zhou and L. Jiang, "Modern description of rayleigh's criterion," *Phys. Rev. A* **99**, 013808 (2019).
- F. Albarelli, M. Barbieri, M. Genoni, and I. Gianani, "A perspective on multiparameter quantum metrology: From theoretical tools to applications in quantum imaging," *Phys. Lett. A* **384**, 126311 (2020).
- W. X. C. D. Y. B. and N. H., "Statistical precision in super-resolution optical fluctuation imaging," *Appl. Opt.* **55**, 7911–7916 (2016).
- W. Vandenberg, M. Leutenegger, S. Duwé, and P. Dedecker, "An extended quantitative model for super-resolution optical fluctuation imaging (sofi)," *Opt. Express* **27**, 25749–25766 (2019).
- S. M. Kay, *Fundamentals of statistical signal processing: estimation theory* (Prentice Hall, 1993).

29. R. M. Dickson, A. B. Cubitt, R. Y. Tsien, and W. E. Moerner, "On/off blinking and switching behaviour of single molecules of green fluorescent protein," *Nature* **388**, 355–358 (1997).
30. A. L. Efros and D. J. Nesbitt, "Origin and control of blinking in quantum dots," *Nat. Nanotechnol.* **11**, 661 (2016).
31. T. Dertinger, R. Colyer, R. Vogel, J. Enderlein, and S. Weiss, "Achieving increased resolution and more pixels with superresolution optical fluctuation imaging (sofi)," *Opt. Express* **18**, 18875–18885 (2010).
32. M. Rosenblatt, "A central limit theorem and a strong mixing condition," *Proc. Natl. Acad. Sci.* **42**, 43–47 (1956).

Super-resolution Optical Fluctuation Imaging—a fundamental estimation theory perspective: supplemental document

1. DETAILS OF FISHER INFORMATION COMPUTATIONS

A detailed derivation of the FI associated with the estimation of the distance between two point sources in different scenarios will be provided in this section. We will start with the simplest, well known case of non-fluctuating Poissonian sources to justify Eq. (4) from the main text. Afterwards, intensity fluctuations will be added to our scheme. Simplified fluctuations model, in which subsequent frames are independent will be examined. We are going to derive a very general formula for FI, which is suitable for different types of intensity fluctuations, not only for two-level emitters presented in the main text. Then, adequate simplifications will be made to obtain the formula for ζ_{\max} (Eq. (8), (9), (10)). In the last part of this section, calculations of the FI associated with different cumulant based algorithms, for both simplified, and realistic Markov-process based model, will be described.

Consider two point emitters placed at $-\theta/2$ and $\theta/2$. The PSF of the imaging system is assumed to be Gaussian with a standard deviation σ :

$$U(x) = (2\pi\sigma^2)^{-1/2} \exp\left(-\frac{x^2}{2\sigma^2}\right). \quad (\text{S1})$$

Our goal is to compute the FI per one photon $\mathcal{F}(\theta)$. To do so, one needs to compute the FI for the whole measurement $\mathcal{F}_{\text{meas}}(\theta)$ and then divide it by the average total number of photons. Our task becomes slightly easier if the whole measurement output can be divided into independent, identically distributed parts (e.g. intensities measured in different, independent frames). It's then enough to compute the FI associated with only one of such independent parts because FI is additive for independent random variables.

A. Non-fluctuating emitters

This case is particularly easy because subsequent photons are not correlated, and the FI per one photon can be calculated directly. Sources are equally bright, and the spatial resolution of the detector is infinite. Each photon position x is independently drawn from the probability density function (PDF):

$$p_{\theta}(x) = \frac{U(x + \theta/2) + U(x - \theta/2)}{2}. \quad (\text{S2})$$

Now the FI can be computed with the help of Eq. (3) in which vector N consists of just one element—a detected photon position x . The \mathcal{F} can be therefore expressed as an integral

$$\mathcal{F}(\theta) = \int_{-\infty}^{\infty} \frac{1}{p_{\theta}(x)} \left(\frac{\partial p_{\theta}(x)}{\partial \theta} \right)^2 dx, \quad (\text{S3})$$

which after substituting the Gaussian form of $U(x)$ simplifies to

$$\sigma^2 \mathcal{F}(\theta) = \frac{1}{4} - \int_{-\infty}^{\infty} \frac{x^2 \exp\left(-\frac{1}{8\sigma^2}(\theta - 2x)^2\right)}{2\sigma^3 \sqrt{2\pi} (\exp(\theta x/\sigma^2) + 1)} dx. \quad (\text{S4})$$

To obtain the analytical form of the above integral for $\theta \ll \sigma$, one can expand the integrated function in the series around $\theta = 0$, and perform the integration term by term to conclude that

$$\mathcal{F}(\theta) = \frac{1}{\sigma^2} \left(\frac{\theta^2}{8\sigma^2} - \frac{\theta^4}{16\sigma^4} + \frac{\theta^6}{24\sigma^6} + \dots \right), \quad (\text{S5})$$

which is consistent with Eq. (4). In order to obtain the values of $\mathcal{F}(\theta)$ for larger θ , the introduced integral must be calculated numerically. To compute \mathcal{F} in case of non-zero pixel size Δx , one needs to construct vector N which consists of mean values of the signal in different pixels only, and then proceed as in subsection C.

B. Fluctuating emitters, independent frames

For the rest of this section, the assumption $\sigma = 1$ will be made. Let's consider the simplified model of fluctuations which is slightly more general than the one described in the main text. In each independent frame relative brightness of emitters placed at $-\theta/2$ and $\theta/2$, denoted by q_1 and q_2 respectively, is independently drawn from the same probability distribution $P(q_i)$. The frame time and the mean emitters power are denoted by τ and \bar{P} respectively—for the sake of simplicity we are going to use the quantity $\bar{n} = \bar{P}\tau$, which is the only relevant quantity as long as frames are independent, and is proportional to the mean number of photons detected per frame. Let's assume for a moment, that relative brightness q_1 and q_2 are fixed and known. The number of photons collected in a given frame from the i -th emitter n_i is then described by the Poisson distribution with the mean value $\langle n_i | q_1, q_2 \rangle = q_i \bar{n}$. The total number of photons n in the frame is therefore described by the distribution $n | q_1, q_2 \sim \text{Poiss}((q_1 + q_2) \bar{n})$. If n, q_1, q_2 are fixed, the PDF of measuring a given sequence of photons positions x_1, \dots, x_n can be written as

$$p_\theta(x_1, \dots, x_n | q_1, q_2, n) = \prod_{i=1}^n p_\theta(x_i | q_1, q_2), \quad (\text{S6})$$

where

$$p_\theta(x_i | q_1, q_2) = \frac{q_1 U(x_i + \theta/2) + q_2 U(x_i - \theta/2)}{q_1 + q_2}. \quad (\text{S7})$$

The above formulas reflect the fact, that subsequent photons positions are uncorrelated if brightness are fixed, and the probability that a given detected photon was emitted from a given source is proportional to its brightness. In reality, one doesn't have a direct access to relative brightness values q_1, q_2 . The observed PDF is averaged over unknown brightness:

$$p_\theta(x_1, \dots, x_n | n) = \int dq_1 \int dq_2 p_\theta(x_1, \dots, x_n | n, q_1, q_2) P(q_1, q_2 | n), \quad (\text{S8})$$

where the conditional probability $P(q_1, q_2 | n)$ is calculated using Bayes' formula:

$$P(q_1, q_2 | n) = \frac{P(n | q_1, q_2) P(q_1) P(q_2)}{P(n)}. \quad (\text{S9})$$

Let's notice that photons positions drawn from the PDF (S8) are correlated within a single frame—correlations arise when the information about brightness is hidden. The information about the total number of photons per frame n is of course available, so it's possible to calculate the FI per frame for each fixed n separately ($\mathcal{F}_{(n)}$), and then compute the FI per one photon using the formula

$$\mathcal{F} = \frac{\langle \mathcal{F}_{(n)} \rangle_n}{\langle n \rangle_n}, \quad (\text{S10})$$

where $\langle X(n) \rangle_n \equiv \sum_n X(n) P(n)$ denotes averaging over n . We are now going to find an expression for $p_\theta(x_1, \dots, x_n | n)$ to compute $\mathcal{F}_{(n)}$ directly from the definition of FI. To do so, let's begin with inserting Eq. (S7) and Eq. (S1) into Eq. (S6). Before performing the product in Eq. (S6), we expand each factor into series around $\theta = 0$. After keeping only the leading terms, we obtain

$$p_\theta(x_1, \dots, x_n | n, q_1, q_2) = (2\pi)^{-n/2} \left(\prod_{i=1}^n e^{-\frac{1}{8} x_i^2} \right) \left(1 + A_1 \theta + A_2 \theta^2 + A_3 \theta^3 + A_4 \theta^4 + \dots \right), \quad (\text{S11})$$

where

$$A_2 = \frac{1}{8} \sum_{i=1}^n x_i^2 + \frac{Q_2}{4} \sum_{i < j} x_i x_j - \frac{1}{8} n, \quad (\text{S12})$$

$$A_4 = \frac{1}{384} \sum_{i=1}^n x_i^4 - \frac{n}{64} \sum_{i=1}^n x_i^2 + \frac{1}{128} n^2 + \frac{Q_2}{96} \sum_{i \neq j} x_i (x_j^3 - 3x_j) + \frac{1}{64} \sum_{i < j} x_i^2 x_j^2 + \frac{Q_2}{32} \sum_{i < j, k \neq i, k \neq j} x_i x_j (x_k^2 - 1) + \frac{Q_4}{16} \sum_{i < j < k < m} x_i x_j x_k x_m, \quad (\text{S13})$$

and the quantity Q_k is defined as

$$Q_k \equiv \left(\frac{q_1 - q_2}{q_1 + q_2} \right)^k. \quad (\text{S14})$$

We don't specify the form of A_1 and A_3 , which are not relevant as will be argued below. Now we can use Eq. (S8) and Eq. (S11) to obtain $p_\theta(x_1, \dots, x_n | n)$. Let us denote the expected value of a function $X(q_1, q_2)$ with respect to $P(q_1, q_2 | n)$ by $\langle X \rangle_{q|n}$:

$$\langle X \rangle_{q|n} \equiv \int X(q_1, q_2) P(q_1, q_2 | n) dq_1 dq_2. \quad (\text{S15})$$

Notice, that if we replace all Q_k terms in Eq. (S12) and Eq. (S13) by their mean values $\langle Q_k \rangle_{q|n}$, we obtain the mean values of coefficients— $\langle A_2 \rangle_{q|n}$ and $\langle A_4 \rangle_{q|n}$. Furthermore:

$$p_\theta(x_1, \dots, x_n | n) = (2\pi)^{-n/2} \left(\prod_{i=1}^n e^{-\frac{1}{8} x_i^2} \right) \left(1 + \langle A_2 \rangle_{q|n} \theta^2 + \langle A_4 \rangle_{q|n} \theta^4 + \mathcal{O}(\theta^6) \right). \quad (\text{S16})$$

We have just used the fact that odd coefficients A_1, A_3, A_5, \dots contain only terms proportional to Q_l , where l is odd. Moreover, from statistical identity of both sources it follows that $\langle Q_l \rangle_{q|n} = 0$ for odd l —that's the reason why odd coefficient could have been neglected from the beginning, and only even θ powers are present in Eq. (S16). We are now going to calculate $\mathcal{F}_{(n)}$ using Eq. (3) which takes the form

$$\mathcal{F}_{(n)} = \int \frac{1}{p_\theta(x_1, \dots, x_n | n)} \left(\frac{\partial p_\theta(x_1, \dots, x_n | n)}{\partial \theta} \right)^2 dx_1 \dots dx_n, \quad (\text{S17})$$

which simplifies to

$$\mathcal{F}_{(n)} = (2\pi)^{-n/2} \int \prod_{i=1}^n e^{-\frac{1}{8} x_i^2} \left(4 \langle A_2 \rangle_{q|n}^2 \theta^2 + \left(16 \langle A_2 \rangle_{q|n} \langle A_4 \rangle_{q|n} - 4 \langle A_2 \rangle_{q|n}^3 \right) \theta^4 + \mathcal{O}(\theta^6) \right) dx_1 \dots dx_n. \quad (\text{S18})$$

After inserting the formulas for $\langle A_2 \rangle_{q|n}$ and $\langle A_4 \rangle_{q|n}$, and performing the integration, we obtain

$$\mathcal{F}_{(n)} = \theta^2 \left[\frac{n}{8} + \frac{\langle Q_2 \rangle_{q|n}^2}{8} n(n-1) \right] + \theta^4 \left[-\frac{n}{16} - \frac{\langle Q_2 \rangle_{q|n}^2}{16} n(n-1) - \frac{\langle Q_2 \rangle_{q|n}^3}{16} n(n-1)(n-2) \right] + \mathcal{O}(\theta^6). \quad (\text{S19})$$

Notice, that now $\theta \ll 1$ condition is not sufficient to ensure that the term with θ^4 is negligible compared to the θ^2 term, because the powers of n are different in both terms. The approximation

$$\mathcal{F}_{(n)} \simeq \theta^2 \left[\frac{n}{8} + \frac{\langle Q_2 \rangle_{q|n}^2}{8} n(n-1) \right] \quad (\text{S20})$$

is nevertheless justified provided $\theta^4 n^3 \ll \theta^2 n^2$, which is equivalent to the condition $\theta \ll n^{-1/2}$. The above inequality holds for all n that give relevant contribution to the final result if $\theta \ll \bar{n}^{-1/2}$. Eq. (S10) allows us to compute the one-photon FI:

$$\mathcal{F} = \frac{\theta^2}{8} \left[1 + \frac{\langle \langle Q_2 \rangle_{q|n}^2 n(n-1) \rangle_n}{\langle n \rangle_n} \right] + \mathcal{O}(\theta^4 \bar{n}^2). \quad (\text{S21})$$

Note that if emitters don't fluctuate, q_1 is always equal to q_2 , so $\langle Q_2 \rangle_{q|n} = 0$, and we recover Eq. (S5) up to the 2nd order of θ —using Eq. (S19) one can additionally check that the coefficient at θ^4 for non-fluctuating case is also correctly retrieved. The quantity $\langle Q_2 \rangle_{q|n}$ can be regarded as

a measure of fluctuations intensity—it becomes larger, if the normalized difference between q_1 and q_2 takes large values with high probability. As intuitively expected, the FI per one photon increases with $\langle Q_2 \rangle_{q|n}$, as well as PRG defined in Eq. (5), which in our case has a form

$$\zeta_{\max} = \left(1 + \frac{\langle \langle Q_2 \rangle_{q|n}^2 n(n-1) \rangle_n}{\langle n \rangle_n} \right)^{1/4}. \quad (\text{S22})$$

In order to obtain a more specific expression for ζ_{\max} , let's consider the two-level model of emitters mentioned in the main text, i.e.

$$P(q_i = q_{\text{off}}) = p \quad (\text{S23})$$

$$P(q_i = q_{\text{on}}) = 1 - p \quad (\text{S24})$$

for $i \in \{1, 2\}$. Recall that $q_{\text{off}} + q_{\text{on}} = 1$, and the fluctuation strength is defined as $\alpha = 1 - q_{\text{off}}/q_{\text{on}}$. It's easy to show that the mean number of photons detected per frame is

$$\langle n \rangle_n = 2\bar{n} \left(p^2 q_{\text{off}} + p(1-p) + (1-p)^2 q_{\text{on}} \right). \quad (\text{S25})$$

The variable Q_2 takes a non-zero value only in two equally probable cases when $q_1 \neq q_2$, so

$$\langle Q_2 \rangle_{q|n} = 2(q_{\text{on}} - q_{\text{off}})^2 P(q_1 = q_{\text{on}}, q_2 = q_{\text{off}}|n). \quad (\text{S26})$$

The probability $P(q_1 = q_{\text{on}}, q_2 = q_{\text{off}}|n)$ is calculated using Eq. (S9), and the fact that

$$P(n|q_1, q_2) = \frac{(\bar{n}(q_1 + q_2))^n \exp(-\bar{n}(q_1 + q_2))}{n!}. \quad (\text{S27})$$

The expression present in Eq. (S22) can be written as an infinite sum

$$\langle \langle Q_2 \rangle_{q|n}^2 n(n-1) \rangle_n = \sum_{n=0}^{\infty} \langle Q_2 \rangle_{q|n}^2 n(n-1) P(n), \quad (\text{S28})$$

which after inserting Eq. (S26) and making some simplifications (e.g. changing variables $q_{\text{on}}, q_{\text{off}}$ to α) takes the form

$$\langle \langle Q_2 \rangle_{q|n}^2 n(n-1) \rangle_n = 4p^2(1-p)^2 \left(\frac{\alpha}{2-\alpha} \right)^4 \bar{n}^2 S, \quad (\text{S29})$$

where

$$S = \sum_{n=0}^{\infty} \frac{e^{-\bar{n}} \bar{n}^n}{n!} \left(B e^{A\bar{n}} (1-A)^n + C + D e^{-A\bar{n}} (1+A)^n \right)^{-1}, \quad (\text{S30})$$

and the following definitions are used: $A = \frac{\alpha}{2-\alpha}$, $B = p^2(1-A)^2$, $C = 2p(1-p)$, $D = (1-p)^2(1+A)^2$. Joining together Eq. (S29), (S25), and (S22), we obtain the following expression:

$$\zeta_{\max} = \left(1 + \frac{2p^2(1-p)^2 \alpha^4}{(2-\alpha)^3(1-p\alpha)} S \bar{n} \right)^{1/4}. \quad (\text{S31})$$

To obtain the value of ζ_{\max} for arbitrary parameters, one needs to approximate the infinite sum S numerically. However, it's possible to prove that (see subsection D)

$$\lim_{\bar{n} \rightarrow \infty} S = \begin{cases} C^{-1} & 0 < \alpha \leq 1 \\ (B + C + D)^{-1} & \alpha = 0 \end{cases}, \quad (\text{S32})$$

which allows us to provide an analytical expression for ζ_{\max} scaling in the infinitely bright sources regime:

$$\lim_{\bar{n} \rightarrow \infty} \zeta_{\max} \bar{n}^{-1/4} = \left(\frac{p(1-p)\alpha^4}{(2-\alpha)^3(1-p\alpha)} \right)^{1/4}. \quad (\text{S33})$$

Numerical analysis show, that the replacement of S by C^{-1} in Eq. (S31), which leads to equation

$$\zeta_{\max} \simeq \left(1 + \frac{p(1-p)\alpha^4}{(2-\alpha)^3(1-p\alpha)} \bar{n} \right)^{1/4} = (1 + G(p, \alpha, \bar{P}\tau) \bar{P}\tau)^{1/4}, \quad (\text{S34})$$

becomes a good approximation for large enough \bar{n} . The comparison between ζ_{\max} computed numerically for finite \bar{n} using Eq. (S31) and its analytical approximation valid for large \bar{n} Eq. (S34) is shown in Fig. S1.

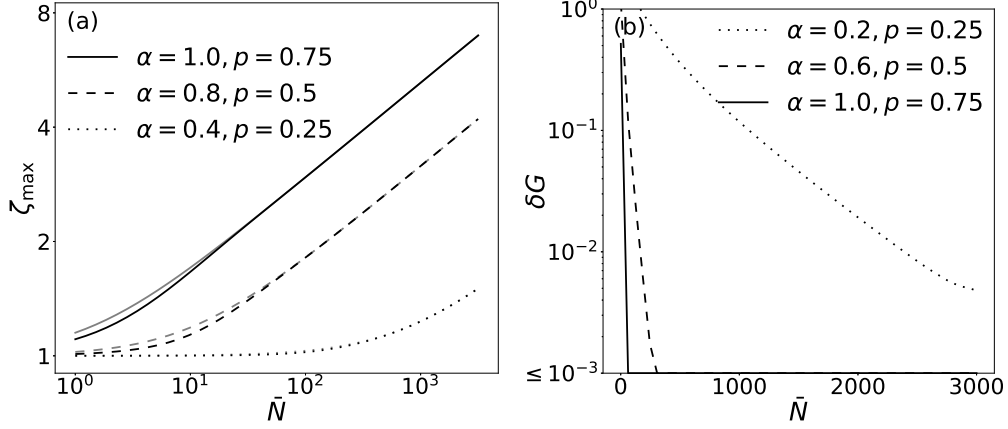


Fig. S1. The comparison between $\zeta(\bar{n})$ computed numerically (black lines), and its analytical approximation (gray lines) for different p and α values is shown in (a). The relative error $\delta G = \frac{G(p,\alpha,\infty) - G(p,\alpha,\bar{n})}{G(p,\alpha,\bar{n})}$ as a function of \bar{n} is sketched in (b).

C. Cumulant based algorithms

From now on the spatial resolution of the camera is not assumed to be infinite, and the whole detection area is divided into M_{pix} pixels of size Δx . The positions of the centroids of subsequent pixels are denoted by $x_1, \dots, x_{M_{\text{pix}}}$. The detection time is divided into M_{fr} frames, m -th frame covers the time interval $[(m-1)\tau, m\tau]$, where $m \in \{1, 2, \dots, M_{\text{fr}}\}$. We are going to consider only two-level blinking model, and stay with its simplified version with independent frames for a while. Our goal is to compute the FI associated with different choices of vector N . Let's consider the case studied in the main text, in which N is described by Eq. (6). Subsequent frames are independent, so the central limit theorem can be directly used to prove that N is normally distributed.

One needs to use slightly more subtle arguments to extend the above reasoning to the estimation based on 2nd auto-cumulant only (AC2). N consists of 2nd auto-cumulant (variance) estimators for each pixel

$$\mathbf{v}_m = \left[n_{1,m}^2 - \langle n_1 \rangle^2, \dots, n_{M_{\text{pix}},m}^2 - \langle n_{M_{\text{pix}}} \rangle^2 \right]^T, \quad (\text{S35})$$

where $\langle n_i \rangle = \frac{1}{M_{\text{fr}}} \sum_{m=1}^{M_{\text{fr}}} n_{i,m}$ denotes the mean value estimator. Unfortunately, this estimator depends on detected photon numbers from different frames, so vectors \mathbf{v}_m are not mutually independent anymore. However, in the limit $M_{\text{fr}} \rightarrow \infty$ the mean value estimator becomes very accurate compared to the variability of the number of photons in a given pixel in a single frame because the variance of $n_{i,m}$ doesn't depend on M_{fr} , and the variance of $\langle n_i \rangle$ scales as $1/M_{\text{fr}}$. That means, that the replacement of the mean value estimator with its exact value in \mathbf{v}_m doesn't affect the distribution of N in the limit $M_{\text{fr}} \rightarrow \infty$. Vectors \mathbf{v}_m become independent after making the described replacement, which allows us to conclude, that N is normally distributed.

In order to compute the FI associated with the normally distributed vector N in the most general case in which both the mean vector $\boldsymbol{\mu}$, and the covariance matrix $\boldsymbol{\Sigma}$ depend on the estimated parameter θ , one can use the formula [1]

$$\mathcal{F}_{(\text{meas})} = \frac{\partial \boldsymbol{\mu}^\top}{\partial \theta} \boldsymbol{\Sigma}^{-1} \frac{\partial \boldsymbol{\mu}}{\partial \theta} + \frac{1}{2} \text{tr} \left(\boldsymbol{\Sigma}^{-1} \frac{\partial \boldsymbol{\Sigma}}{\partial \theta} \boldsymbol{\Sigma}^{-1} \frac{\partial \boldsymbol{\Sigma}}{\partial \theta} \right). \quad (\text{S36})$$

If vectors \mathbf{v}_m are independent and identically distributed (i.i.d.), the mean vector and the covariance matrix for each \mathbf{v}_m are denoted by $\boldsymbol{\mu}_{(1)}$ and $\boldsymbol{\Sigma}_{(1)}$, then $\boldsymbol{\mu} = \boldsymbol{\mu}_{(1)}$, and $\boldsymbol{\Sigma} = \frac{1}{M_{\text{fr}}} \boldsymbol{\Sigma}_{(1)}$. We therefore see, that the 2nd term in Eq. (S36) is negligible compared to the 1st term in the limit $M_{\text{fr}} \rightarrow \infty$ (provided the first term is non-zero), and hence in this limit we may write

$$\mathcal{F}_{(\text{meas})} = \frac{\partial \boldsymbol{\mu}^\top}{\partial \theta} \boldsymbol{\Sigma}^{-1} \frac{\partial \boldsymbol{\mu}}{\partial \theta} = M_{\text{fr}} \frac{\partial \boldsymbol{\mu}_{(1)}^\top}{\partial \theta} \boldsymbol{\Sigma}_{(1)}^{-1} \frac{\partial \boldsymbol{\mu}_{(1)}}{\partial \theta}. \quad (\text{S37})$$

In order to compute the FI per one photon \mathcal{F} one needs to compute the elements of $\boldsymbol{\mu}$ and $\boldsymbol{\Sigma}$, use Eq. (S37), and then divide $\mathcal{F}_{(\text{meas})}$ by the average total photon number. Let $v_{1,m}, v_{2,m}, \dots, v_{n,m}$ be the elements of the vector \boldsymbol{v}_m . In some cases we are going to use a short-hand notation $v_{i,1} \equiv v_i, n_{i,1} \equiv n_i$, because the 2nd index can be omitted in many situations when single frame statistics are considered. Then:

$$\boldsymbol{\mu} = [\langle v_1 \rangle, \langle v_2 \rangle, \dots, \langle v_n \rangle]^T, \quad (\text{S38})$$

$$\boldsymbol{\Sigma} = \frac{1}{M_{\text{fr}}} \left(\begin{array}{c} \left[\begin{array}{cccc} \langle v_1 v_1 \rangle & \langle v_1 v_2 \rangle & \dots & \langle v_1 v_n \rangle \\ \langle v_2 v_1 \rangle & \langle v_2 v_2 \rangle & \dots & \langle v_2 v_n \rangle \\ \vdots & \vdots & \ddots & \vdots \\ \langle v_n v_1 \rangle & \langle v_n v_2 \rangle & \dots & \langle v_n v_n \rangle \end{array} \right] - \boldsymbol{\mu} \boldsymbol{\mu}^T \end{array} \right). \quad (\text{S39})$$

In every considered case each v_i ($i \in \{1, 2, \dots, n\}$) can be written as a linear combination of elements of the form $n_j^{k_1} n_l^{k_2}$ where $j, l \in \{1, 2, \dots, M_{\text{pix}}\}$, and k_1, k_2 are natural exponents (possibly zero). Therefore, it's enough to be able to compute expected values of products $\langle n_{j_1}^{k_1} n_{j_2}^{k_2} \dots n_{j_r}^{k_r} \rangle$ for $r \leq 4$ to reconstruct all terms of $\boldsymbol{\mu}$ and $\boldsymbol{\Sigma}$. The procedure used to compute these expected values is as follows. PSFs of both sources are numerically integrated over different pixels—we construct variables

$$U_{j,1} = \int_{x_j - \Delta x/2}^{x_j + \Delta x/2} U(x + \theta/2) dx, \quad U_{j,2} = \int_{x_j - \Delta x/2}^{x_j + \Delta x/2} U(x - \theta/2) dx, \quad (\text{S40})$$

where $j \in \{1, 2, \dots, M_{\text{pix}}\}$ denotes the pixel label. Now we use the fact, that the number of photons detected in each pixel, when the sources brightness are fixed, is described by a Poisson distribution with a mean value

$$\langle n_j | q_1, q_2 \rangle = (q_1 U_{j,1} + q_2 U_{j,2}) \bar{n}, \quad (\text{S41})$$

where $q_1, q_2 \in \{q_{\text{off}}, q_{\text{on}}\}$ denote relative brightness of the 1st and the 2nd emitter respectively. Moreover, conditional random variables $n_j | q_1, q_2$ are mutually independent, so the expected value of a product of their powers is:

$$\langle n_{j_1}^{k_1} n_{j_2}^{k_2} \dots n_{j_r}^{k_r} | q_1, q_2 \rangle = \prod_{i=1}^r M_{k_i}(\langle n_{j_i} | q_1, q_2 \rangle), \quad (\text{S42})$$

where $M_k(v)$ denotes a k -th raw moment of Poisson distribution with a mean value v , e.g. $M_0(v) = 1, M_1(v) = v, M_2(v) = v^2 + v, M_3(v) = v^3 + 3v^2 + v, M_4(v) = v^4 + 6v^3 + 7v^2 + v$. Eq. (S42) is only valid if indices j_1, \dots, j_r are mutually different—if any index repeats, one should replace an expression of the form $n_j^{k_1} n_j^{k_2}$ with an expression $n_j^{k_1+k_2}$, repeat such a procedure as long as there are any repetitions left, and only then use Eq. (S42) directly. Already described steps allow us to compute conditional expected values. In order to compute the desired expected values $\langle n_{j_1}^{k_1} n_{j_2}^{k_2} \dots n_{j_r}^{k_r} \rangle$ one only needs to average the conditional ones over four different configurations of the emitters using the formula

$$\langle X \rangle = p^2 \langle X | q_{\text{off}}, q_{\text{off}} \rangle + p(1-p) (\langle X | q_{\text{off}}, q_{\text{on}} \rangle + \langle X | q_{\text{on}}, q_{\text{off}} \rangle) + (1-p)^2 \langle X | q_{\text{on}}, q_{\text{on}} \rangle. \quad (\text{S43})$$

By performing the described steps numerically, we obtain $\mathcal{F}(\theta)$ (and consequently ζ) associated with different image reconstruction algorithms in the simplified blinking model.

We will now show, how to extend this scheme to the case of Markov process based realistic model. Let's first remind, that the relative brightness of each emitter is described by a Markov process with two possible states with different relative brightness: q_{on} and q_{off} . The brightness of each emitter is a function of time $P_i(t)$ ($i \in \{1, 2\}$), which takes two possible values: $q_{\text{off}} \bar{P}, q_{\text{on}} \bar{P}$. During a short time interval $[t, t + \delta t]$ i -th emitter emits $P_i(t) \delta t$ photons on average. Lifetimes of on- and off- states are equal to τ_{off} and τ_{on} respectively. The probability that a given emitter remains in a fixed state with a lifetime τ_i for a time period t is proportional to $\exp(-t/\tau_i)$. Let's

now introduce a more formal description of the Markov process, which leads to such an exponential behaviour. At any time t , the state of an emitter is described by a vector $\begin{bmatrix} p_{\text{off}} \\ p_{\text{on}} \end{bmatrix}$, where p_{off} and p_{on} denote the probabilities of finding the emitter in off- and on- state respectively. The time evolution of the emitter state is given by

$$\begin{bmatrix} p_{\text{off}} \\ p_{\text{on}} \end{bmatrix} (t + \Delta t) = \mathbf{T}(\Delta t) \begin{bmatrix} p_{\text{off}} \\ p_{\text{on}} \end{bmatrix} (t), \quad (\text{S44})$$

where $\mathbf{T}(\Delta t)$ is a transition matrix defined as

$$\mathbf{T}(\Delta t) = \begin{bmatrix} t_{00} & t_{10} \\ t_{01} & t_{11} \end{bmatrix} (\Delta t) = \exp \left(\Delta t \begin{bmatrix} -\tau_{\text{off}}^{-1} & \tau_{\text{on}}^{-1} \\ \tau_{\text{off}}^{-1} & -\tau_{\text{on}}^{-1} \end{bmatrix} \right). \quad (\text{S45})$$

It's easy to check, that after a long evolution the state always converges to

$$\begin{bmatrix} p_{\text{off}} \\ p_{\text{on}} \end{bmatrix} (\Delta t \rightarrow \infty) = \begin{bmatrix} \tilde{p}_{\text{off}} \\ \tilde{p}_{\text{on}} \end{bmatrix} = \frac{1}{\tau_{\text{off}} + \tau_{\text{on}}} \begin{bmatrix} \tau_{\text{off}} \\ \tau_{\text{on}} \end{bmatrix}. \quad (\text{S46})$$

$\begin{bmatrix} \tilde{p}_{\text{off}} \\ \tilde{p}_{\text{on}} \end{bmatrix}$ is a stationary state of the process, and will be used as an initial state in our considerations— if no information about the previous run of the process is available, the probability of finding an emitter in a given state is proportional to its lifetime. Using the transition matrix $\mathbf{T}(\Delta t)$ elements, let's define the $\mathbf{S}(\Delta t)$ matrix:

$$\mathbf{S}(\Delta t) = \begin{bmatrix} t_{00}(\Delta t)q_{\text{off}}\bar{P} & t_{01}(\Delta t)q_{\text{off}}\bar{P} \\ t_{10}(\Delta t)q_{\text{on}}\bar{P} & t_{11}(\Delta t)q_{\text{on}}\bar{P} \end{bmatrix}, \quad (\text{S47})$$

which allows us to write down formulas for temporal brightness correlations in a compact way:

$$\langle P_i(t_1)P_i(t_2)\dots P_i(t_r) \rangle = \begin{bmatrix} \tilde{p}_{\text{off}} & \tilde{p}_{\text{on}} \end{bmatrix} \mathbf{S}(t_2 - t_1)\mathbf{S}(t_3 - t_2)\dots\mathbf{S}(t_r - t_{r-1}) \begin{bmatrix} q_{\text{off}}\bar{P} \\ q_{\text{on}}\bar{P} \end{bmatrix}. \quad (\text{S48})$$

In the above formula $t_1 \leq t_2 \leq \dots \leq t_r$, and $\langle \bullet \rangle$ denotes averaging over Markov processes $P_1(t)$, $P_2(t)$. Two emitters are independent, so in order to compute a product in which P_1 and P_2 terms are mixed, one can use the formula

$$\langle \mathcal{G}_1 [P_1(t)] \mathcal{G}_2 [P_2(t)] \rangle = \langle \mathcal{G}_1 [P_1(t)] \rangle \langle \mathcal{G}_2 [P_2(t)] \rangle, \quad (\text{S49})$$

which is true for all functionals $\mathcal{G}_1, \mathcal{G}_2$. Further on, the following integrals of correlations over detection time frames will be useful:

$$\chi_1 = \int_0^\tau \langle P_i(t) \rangle dt = \langle P_i \rangle \tau \quad (\text{S50})$$

$$\chi_{2,m} = \int_0^\tau dt_1 \int_{(m-1)\tau}^{m\tau} dt_2 \langle P_i(t_1)P_i(t_2) \rangle \quad (\text{S51})$$

$$\chi_{3,m} = \int_0^\tau dt_1 \int_0^\tau dt_2 \int_{(m-1)\tau}^{m\tau} dt_3 \langle P_i(t_1)P_i(t_2)P_i(t_3) \rangle \quad (\text{S52})$$

$$\chi_{4,m} = \int_0^\tau dt_1 \int_0^\tau dt_2 \int_{(m-1)\tau}^{m\tau} dt_3 \int_{(m-1)\tau}^{m\tau} dt_4 \langle P_i(t_1)P_i(t_2)P_i(t_3)P_i(t_4) \rangle \quad (\text{S53})$$

At this point, we are prepared to attack the problem of computing \mathcal{F} . Although the frames are now correlated, we still consider vectors \mathbf{N} that can be written as in Eq. (6), and we can use the central limit theorem in its extended version [2] because correlations between frames decay exponentially with time. Therefore, it's again enough to calculate $\boldsymbol{\mu}$ and $\boldsymbol{\Sigma}$ associated with \mathbf{N} , and then use Eq. (S36). The scaling of both terms in this equation remains the same, so the 2nd

term again disappears in the limit $M_{\text{fr}} \rightarrow \infty$. Eq. (S38) is still valid, and can be used to calculate $\boldsymbol{\mu}$, but in order to compute $\boldsymbol{\Sigma}$ elements one needs to take into account correlations between frames:

$$\boldsymbol{\Sigma}_{ij} = \frac{1}{M_{\text{fr}}^2} \sum_{m, m'=1}^{M_{\text{fr}}} \text{cov}(v_{i,m}, v_{j,m'}). \quad (\text{S54})$$

In the limit $M_{\text{fr}} \rightarrow \infty$, using the homogeneity of the Markov processes, we can simplify our formula:

$$\boldsymbol{\Sigma}_{ij} = \frac{1}{M_{\text{fr}}} \left(\text{cov}(v_{i,1}, v_{j,1}) + 2 \sum_{m=2}^{\infty} \text{cov}(v_{i,1}, v_{j,m}) \right). \quad (\text{S55})$$

Analogously to the previous case, photon numbers in different pixels and time frames are uncorrelated and described by a Poisson distribution if functions $P_1(t), P_2(t)$ are fixed, and we have:

$$\langle n_{j,m} | P_1(t), P_2(t) \rangle \equiv \mu_{j,m} = \int_{(m-1)\tau}^{m\tau} (P_1(t)U_{1,j} + P_2(t)U_{2,j}) dt. \quad (\text{S56})$$

Conditional products of variables $n_{j,m}$ are computed with the help of the formula

$$\langle n_{j_1, m_1}^{k_1} n_{j_2, m_2}^{k_2} \dots n_{j_r, m_r}^{k_r} | P_1(t), P_2(t) \rangle = \prod_{i=1}^r M_{k_i}(\mu_{j_i, m_i}) \quad (\text{S57})$$

valid if pairs (j_i, m_i) mutually differ on at least one position. All terms of $\boldsymbol{\mu}$ and $\boldsymbol{\Sigma}$ are linear combinations of expectation values (where averaging over Markov processes is made) $\langle n_{j_1, m_1}^{k_1} n_{j_2, m_2}^{k_2} \dots n_{j_r, m_r}^{k_r} \rangle$. We want restrict ourselves to N which consist of 2nd order correlations at most, so from now on we assume that $k_1 + k_2 + \dots k_r \leq 4$. Then, after expanding the RHS of Eq. (S57), and using formulas for Poisson distribution moments, we see that all conditional expected values are linear combinations of products of $\mu_{j,m}$ with at most 4 terms. Expectation values required to reconstruct $\boldsymbol{\mu}$ and $\boldsymbol{\Sigma}$ are linear combinations of similar products averaged over Markov processes. Such products can be written with the help of variables χ , defined in Eq. (S50)-(S53),

$$\langle \mu_{j,m} \rangle = (U_{1,j} + U_{2,j})\chi_1, \quad (\text{S58})$$

$$\langle \mu_{j,0}\mu_{j',m} \rangle = (U_{1,j}U_{1,j'} + U_{2,j}U_{2,j'})\chi_{2,m} + (U_{1,j}U_{2,j'} + U_{2,j}U_{1,j'})\chi_1^2, \quad (\text{S59})$$

$$\begin{aligned} \langle \mu_{j,0}\mu_{j',0}\mu_{j'',m} \rangle &= U_{1,j}U_{1,j'}U_{1,j''}\chi_{3,m} + U_{1,j}U_{1,j'}U_{2,j''}\chi_{2,0}\chi_1 + \\ &+ (U_{1,j}U_{2,j'}U_{1,j''} + U_{1,j}U_{2,j'}U_{2,j''})\chi_{2,m}\chi_1 + (1 \leftrightarrow 2), \end{aligned} \quad (\text{S60})$$

$$\begin{aligned} \langle \mu_{j,0}\mu_{j',0}\mu_{j'',m}\mu_{j''',m} \rangle &= U_{1,j}U_{1,j'}U_{1,j''}U_{1,j'''}\chi_{4,m} + \\ &+ (U_{1,j}U_{1,j'}U_{1,j''}U_{2,j'''} + U_{1,j}U_{1,j'}U_{2,j''}U_{1,j'''} + U_{1,j}U_{2,j'}U_{1,j''}U_{1,j'''} + U_{1,j}U_{2,j'}U_{2,j''}U_{2,j'''})\chi_{3,m}\chi_1 + \\ &+ U_{1,j}U_{1,j'}U_{2,j''}U_{2,j'''}\chi_{2,0}^2 + (U_{1,j}U_{2,j'}U_{1,j''}U_{2,j'''} + U_{1,j}U_{2,j'}U_{2,j''}U_{1,j'''})\chi_{2,m}^2 + (1 \leftrightarrow 2). \end{aligned} \quad (\text{S61})$$

Notation $(1 \leftrightarrow 2)$ means that terms with swapped indices 1 and 2, that correspond to the 1st and 2nd emitter, should be added.

Let's summarize the procedure used to compute $\boldsymbol{\mu}$ and $\boldsymbol{\Sigma}$ for the Markov process based model. First, Eqs. (S38) and (S55) are applied, and all terms are expressed as linear combinations of expected values $\langle n_{j_1, m_1}^{k_1} n_{j_2, m_2}^{k_2} \dots n_{j_r, m_r}^{k_r} \rangle$. Then, conditional expected values $\langle n_{j_1, m_1}^{k_1} n_{j_2, m_2}^{k_2} \dots n_{j_r, m_r}^{k_r} | P_1(t), P_2(t) \rangle$ are computed with the help of Eq. (S57). Averaging over Markov processes $P_1(t), P_2(t)$ is made after expanding the RHS of Eq. (S57), formulas (Eq. (S58)-Eq. (S61)) are then utilized to express $\langle n_{j_1, m_1}^{k_1} n_{j_2, m_2}^{k_2} \dots n_{j_r, m_r}^{k_r} \rangle$ using variables $U_{1,j}$, $U_{2,j}$, and χ (Eq. (S50)-(S53)). Notice, that the sum present in Eq. (S58) is infinite, but in our case all sums converge. Moreover, it's possible to express all the terms of $\boldsymbol{\mu}$ and $\boldsymbol{\Sigma}$ in the considered cases with the help of variables $U_{1,j}, U_{2,j}$ (computed numerically), $\chi_1, \chi_{2,1}, \chi_{3,1}, \chi_{4,1}$, and the following infinite sums (all of them converge):

$$S_1 = \sum_{m=2}^{\infty} (\chi_{2,m} - \chi_1^2), \quad (\text{S62})$$

$$S_2 = \sum_{m=2}^{\infty} (\chi_{3,m} - \chi_{2,1}\chi_1), \quad (\text{S63})$$

$$S_3 = \sum_{m=2}^{\infty} (\chi_{4,m} - \chi_{2,1}^2), \quad (\text{S64})$$

$$S_4 = \sum_{m=2}^{\infty} (\chi_{2,m}^2 - \chi_1^4) \quad (\text{S65})$$

where χ variables are expressed as functions of the setup parameters analytically with the help of Eqs.(S48, S50-S53), and then sums S_1, S_2, S_3, S_4 are also computed analytically (they can be expressed as sums of geometric series).

D. Proof of Eq. (S32)

In this section we provide a rigorous proof of Eq. (S32). For $\alpha = 0$, we have $A = 0$, the value of the sum doesn't depend on \bar{n} and can be easily computed, and the proof becomes trivial. For $0 < \alpha \leq 1$ we need to prove that

$$\lim_{\bar{n} \rightarrow \infty} \sum_{n=0}^{\infty} \frac{e^{-\bar{n}} \bar{n}^n}{n!} \left(B e^{A\bar{n}} (1-A)^n + C + D e^{-A\bar{n}} (1+A)^n \right)^{-1} = C^{-1}, \quad (\text{S66})$$

where $0 < A \leq 1, B, D \geq 0, C > 0$. Let us define

$$X_n(\bar{n}) := \frac{e^{-\bar{n}} \bar{n}^n}{n!} \left(B e^{A\bar{n}} (1-A)^n + C + D e^{-A\bar{n}} (1+A)^n \right)^{-1}. \quad (\text{S67})$$

We are going to use the following property of Poisson distribution:

$$\forall \delta > 0, \epsilon > 0 \exists N_0 \forall \bar{n} > N_0 : 0 < \sum_{n=0}^{\infty} \frac{e^{-\bar{n}} \bar{n}^n}{n!} - \sum_{n=(1-\epsilon)\bar{n}}^{(1+\epsilon)\bar{n}} \frac{e^{-\bar{n}} \bar{n}^n}{n!} < \delta. \quad (\text{S68})$$

Intuitively, for large enough \bar{n} , all probable values of Poisson distribution are located in the range $\bar{n}(1 \pm \epsilon)$, because the standard deviation of Poisson distribution with mean \bar{n} is $\sqrt{\bar{n}}$. Let's notice that $X_n(\bar{n}) \leq C^{-1} \frac{\bar{n}^n e^{-\bar{n}}}{n!}$, so the following inequality is true:

$$0 < \sum_{n=0}^{\infty} X_n(\bar{n}) - \sum_{n=(1-\epsilon)\bar{n}}^{(1+\epsilon)\bar{n}} X_n(\bar{n}) \leq C^{-1} \left(\sum_{n=0}^{\infty} \frac{e^{-\bar{n}} \bar{n}^n}{n!} - \sum_{n=(1-\epsilon)\bar{n}}^{(1+\epsilon)\bar{n}} \frac{e^{-\bar{n}} \bar{n}^n}{n!} \right), \quad (\text{S69})$$

which after using Eq. (S68) allows us to conclude that:

$$\forall \epsilon > 0 \lim_{\bar{n} \rightarrow \infty} \sum_{n=0}^{\infty} X_n(\bar{n}) = \lim_{\bar{n} \rightarrow \infty} \sum_{n=(1-\epsilon)\bar{n}}^{(1+\epsilon)\bar{n}} X_n(\bar{n}). \quad (\text{S70})$$

Let's now fix $\epsilon, \delta_1 > 0$ satisfying

$$A + (1-\epsilon) \log(1-A) < -\delta_1, \quad (\text{S71})$$

$$-A + (1+\epsilon) \log(1+A) < -\delta_1. \quad (\text{S72})$$

For $A = 1$ the first inequality may be omitted. It's easy to show, that the described choice of positive constants ϵ and δ_1 is always possible. Such a choice allows us to conclude, that for $n \in [\bar{n}(1-\epsilon), \bar{n}(1+\epsilon)]$:

$$e^{A\bar{n}} (1-A)^n \leq e^{\bar{n}(A+(1-\epsilon)\log(1-A))} < e^{-\delta_1 \bar{n}}, \quad (\text{S73})$$

$$e^{-A\bar{n}} (1+A)^n \leq e^{\bar{n}(-A+(1+\epsilon)\log(1+A))} < e^{-\delta_1 \bar{n}}. \quad (\text{S74})$$

Therefore,

$$1 \leq \left(\frac{e^{-\bar{n}} \bar{n}^n}{C n!} \right) / X_n(\bar{n}) \leq 1 + \frac{B+D}{C} e^{-\delta_1 \bar{n}}, \quad (\text{S75})$$

and consequently

$$\left(1 + \frac{B+D}{C}e^{-\delta_1\bar{n}}\right)^{-1} \sum_{n=(1-\epsilon)\bar{n}}^{(1+\epsilon)\bar{n}} \frac{e^{-\bar{n}}\bar{n}^n}{Cn!} \leq \sum_{n=(1-\epsilon)\bar{n}}^{(1+\epsilon)\bar{n}} X_n(\bar{n}) \leq \sum_{n=(1-\epsilon)\bar{n}}^{(1+\epsilon)\bar{n}} \frac{e^{-\bar{n}}\bar{n}^n}{Cn!}. \quad (\text{S76})$$

Since $e^{-\delta_1\bar{n}} \rightarrow 0$ for $\bar{n} \rightarrow \infty$, and sum $\sum_{n=(1-\epsilon)\bar{n}}^{(1+\epsilon)\bar{n}} \frac{e^{-\bar{n}}\bar{n}^n}{Cn!}$ converges to C^{-1} (as a consequence of Eq. (S68)), we can use the so called *sandwich theorem* to finally conclude that

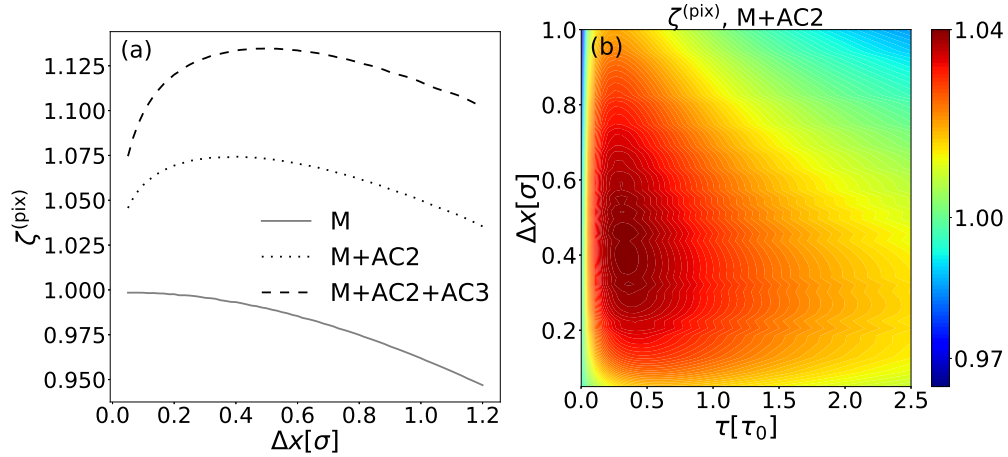
$$\lim_{\bar{n} \rightarrow \infty} \sum_{n=0}^{\infty} X_n(\bar{n}) = \lim_{\bar{n} \rightarrow \infty} \sum_{n=(1-\epsilon)\bar{n}}^{(1+\epsilon)\bar{n}} X_n(\bar{n}) = C^{-1}. \quad (\text{S77})$$

2. THE IMPACT OF THE PIXEL SIZE AND NON-EQUAL STATES PROBABILITIES

The dependence of the \mathcal{F} and ζ on the pixel size was not discussed in the main text—spatial resolution was either assumed to be infinite, or the assumption $\Delta x = 0.5\sigma$ was made. When ζ was computed using Eq. (5), the same pixel size was used to calculate \mathcal{F} and $\mathcal{F}^{(\text{SI})}$. In order to examine the impact of the pixel size for different methods, we will use a slightly modified figure of merit defined as:

$$\zeta^{(\text{pix})} = \lim_{\theta \rightarrow 0} \left(\mathcal{F}(\theta) / \left(\frac{\theta^2}{8\sigma^4} \right) \right)^{1/4}. \quad (\text{S78})$$

This modification fixes the denominator to $\mathcal{F}^{(\text{SI})}$ associated with the infinite spatial resolution of the detector. It allows us to observe, for example, how the Standard Imaging resolution decreases when Δx is too large. The role of the pixel size becomes less trivial when auto-cumulants are used in the estimation (see Fig. S2a). Pixels can't be of course too large, but very small pixels are no longer the optimal choice because the information contained in the correlations between pixels is lost. In particular, higher auto-cumulants don't provide any extra information if one photon per frame per pixel is detected at most. The described problem disappears when cross-cumulants are used, and very small pixels again become advantageous. Notice the fact, that a similar trade-off is observed in the time domain, when one changes the frame time. Very short time frames would only be optimal if correlations between frames were used, but such schemes are not analyzed in this work.



(a) a

Fig. S2. Fig.(a) shows the dependence of $\zeta^{(\text{pix})}$ on the pixel size Δx for auto-cumulant based estimation schemes. If we go beyond the standard approach (M), infinitely small pixels are not optimal. Fig.(b) shows how $\zeta^{(\text{pix})}$ is affected when both Δx and τ changes for 2nd auto-cumulant based estimation (M+AC2). In (a) the simplified model was used ($p = 0.5$, $\bar{P}\tau = 1000$), whereas for (b) Markov process based model with $\tau_{\text{on}} = \tau_{\text{off}} = \tau_0$, and $\bar{P} = 1000\tau_0^{-1}$ was applied. In both cases $\alpha = 0.9$.

The assumption $\tau_{\text{on}} = \tau_{\text{off}}$ (realistic model) or $p = 1/2$ (simplified model) was usually made in the main text. However, it's known that real emitters sometimes break this assumption, and favor one of the states. Fortunately, the procedures described in section 1 don't rely on any assumptions about blinking parameters, so the results for $\tau_{\text{off}} \neq \tau_{\text{on}}$ can be easily obtained. One can then observe, that if off- state is more probable, the PRG becomes higher. One should also take this asymmetry into account while dealing with optimizing the time frame for different estimation schemes—see Fig. S3.

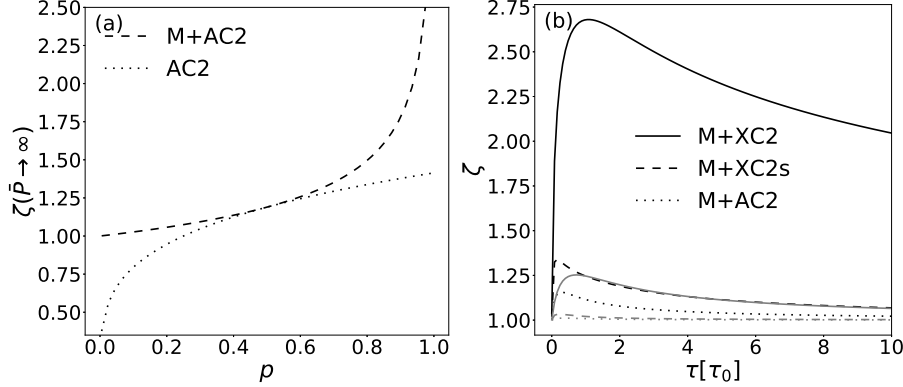


Fig. S3. The PRG in the limit of infinitely bright sources and strong fluctuations ($\alpha = 1$) as a function of $p = P(q_{\text{off}})$ is sketched in (a) (the simplified blinking model is used). One can observe, that estimation schemes based on (AC2) and (M+AC2) are only equivalent for $p = 0.5$. For $p > 0.5$ the PRG can be larger than $\sqrt[4]{2}$, but the (AC2) scheme never allows to beat $\zeta < \sqrt{2}$ limit. The PRGs computed for the realistic model are sketched in (b). Gray lines denote $\tau_{\text{off}} = 0.4\tau_0$, $\tau_{\text{on}} = 1.6\tau_0$ case, whereas $\tau_{\text{off}} = 1.6\tau_0$, $\tau_{\text{on}} = 0.4\tau_0$ for black lines, and $\alpha = 1$ for both cases. A significant increase of ζ is possible, when off- state is favored because more frames in which only one emitter is active are observed.

3. ANTI-BUNCHING BASED SUPER-RESOLUTION

The analysis of the performance of super-resolution microscopy based on the intensity fluctuations of emitters was the main subject of this work. However, the introduced figure of merit ζ can be used for any super-resolution technique. To provide a simple example which can't be described by the already examined intensity fluctuations model, let's consider the super-resolution imaging based on quantum correlations (anti-bunching). As it's believed [3], the resolution can be increased by a factor $\sqrt{2}$ if two emitters are imaged, two-photon frames are observed, and due to anti-bunching phenomenon one can be sure, that at most one photon can be emitted from a single source within a single frame. Let's check this statement by computing the PRG for this case. The geometry of the imaged binary source remains the same. In the most optimistic case, the whole measurement consists of two-photon frames only—in reality, one-photon frames can also be measured, and such frames can't be used to obtain super-resolution. After using the fact, that two photons within a single frame must originate from two different sources, we can write the PDF of measuring two photons at positions x_1, x_2 as:

$$p_{\theta}(x_1, x_2) = \frac{1}{2} (U(x_1 + \theta/2)U(x_2 - \theta/2) + U(x_2 + \theta/2)U(x_1 - \theta/2)) \quad (\text{S79})$$

After substituting the Gaussian form of the PSF U (Eq. (S1)), and fixing $\sigma = 1$, we obtain:

$$p_{\theta}(x_1, x_2) = (4\pi)^{-1} \left(e^{-\frac{1}{2}(\frac{\theta}{2} + x_1)^2 - \frac{1}{2}(x_2 - \frac{\theta}{2})^2} + e^{-\frac{1}{2}(x_1 - \frac{\theta}{2})^2 - \frac{1}{2}(\frac{\theta}{2} + x_2)^2} \right). \quad (\text{S80})$$

The FI per two-photon frame $\mathcal{F}_{(2)}$ is now computed with the help of Eq. (3):

$$\mathcal{F}_{(2)} = \frac{1}{2} - \int_{-\infty}^{\infty} \int_{-\infty}^{\infty} dx_1 dx_2 \frac{(x_1 - x_2)^2 \exp\left(\frac{1}{4}(-\theta^2 + 2\theta x_1 + 2x_2(\theta - x_2) - 2x_1^2)\right)}{4\pi(e^{\theta x_1} + e^{\theta x_2})}. \quad (\text{S81})$$

To compute the FI per single photon (\mathcal{F}) for small θ , one should expand the integrated function in a series around $\theta = 0$, perform the integration term by term, and use the formula

$$\mathcal{F} = \frac{1}{2}\mathcal{F}_{(2)} \quad (\text{S82})$$

to conclude that

$$\mathcal{F}(\theta) = \frac{\theta^2}{4} - \frac{\theta^4}{4} + \frac{\theta^6}{3} + \dots \quad (\text{S83})$$

After using the formula for $\mathcal{F}^{(\text{SI})}$ (Eq. (4)), we easily see that

$$\zeta = \sqrt[4]{2}. \quad (\text{S84})$$

Despite optimistic assumptions, our PRG again turns out to be lower than the resolution gain predicted by the PSF analysis— $\sqrt{2}$ is replaced by $\sqrt[4]{2}$ as in the case of 2nd auto-cumulant based estimation for $p = 1/2$.

REFERENCES

1. S. M. Kay, *Fundamentals of statistical signal processing: estimation theory* (Prentice Hall, 1993).
2. M. Rosenblatt, "A central limit theorem and a strong mixing condition," *Proc. Natl. Acad. Sci.* **42**, 43–47 (1956).
3. O. Schwartz, J. M. Levitt, R. Tenne, S. Itzhakov, Z. Deutsch, and D. Oron, "Superresolution microscopy with quantum emitters," *Nano letters* **13**, 5832–5836 (2013).